Macromolecules

pubs.acs.org/Macromolecules Article

Cooperative Multivalent Weak and Strong Interfacial Interactions Enhance the Adhesion of Mussel-Inspired Adhesives

Amal Narayanan,[#] Sukhmanjot Kaur,[#] Nityanshu Kumar, Mesfin Tsige, Abraham Joy,* and Ali Dhinojwala*

Cite This: *Macromolecules* 2021, 54, 5417−5428 Read Online

ACCESS | Metrics & More | Article Recommendations | Supporting Information

ABSTRACT: Inspired by the strong adhesion of mussel byssal threads to surfaces, the incorporation of 3,4-dihydroxyphenylalanine (DOPA) in polymer architecture has become a popular strategy to improve the adhesion of the polymers. There are numerous literature reports of this bioinspired method to improve the adhesion performance of polymers. However, the mechanism behind the success of DOPA-based adhesion continues to be a puzzle as decoupling the contribution of interfacial adhesion to the alteration in chemistry is experimentally challenging. Herein, we designed mussel-inspired elastomers with four different functionalities to test the importance of aromatic and hydroxyl groups in determining the adhesion performance. With a combination of adhesion measurements, surface-sensitive spectroscopy, and molecular dynamics simulations, we show that the aromatic groups form weak multivalent acid−base interactions with the surface hydroxyl groups on sapphire. Also, the interaction of both phenyl (weak acid−base interaction) and −OH groups (strong acid−base interaction) of DOPA with sapphire −OH groups increases the adhesion of DOPA-based polymers compared to polymer analogs functionalized with either phenylalanine (only aromatic), serine (only hydroxyl), or tyrosine (aromatic and one hydroxyl) groups. Thus, this study illustrates the importance of both strong and weak acid−base interactions in enhancing adhesion.

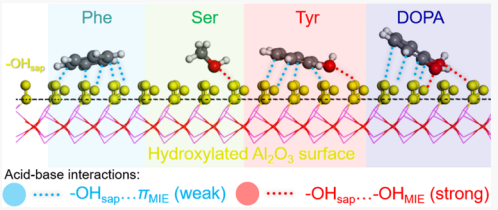

INTRODUCTION

The drive to understand the mechanisms used by living organisms to adhere to surfaces has resulted in the discovery of the chemical and physical contributions of fibrillar adhesives in geckos and insects,[1,2] glycoproteins in slug mucus[3,4] and spider silk adhesives,[5,6] polyelectrolyte complexes in sandcastle worm cement,[7,8] and 3,4-dihydroxyphenylalanine (DOPA) functional groups in mussel foot proteins[9,10] (Mfps). Among these examples, the DOPA functionality in Mfps is arguably the most studied system.[11,12] The unusual presence of DOPA functionality in Mfps is a result of site-specific post-translational modification of tyrosine units.[12] The dihydroxyl groups in DOPA ($-OH_{DOPA}$) chelate with metallic surfaces to form strong bonds even in the presence of water.[13,14] Because mussels stick to diverse surfaces in addition to metals,[15] other intermolecular interactions such as hydrogen bonding,[13,14,16−23] catechol−cation synergy,[22,24−31] dispersive interactions,[20,32,33] and $\pi-\pi$,[32] cation$-\pi$,[34,35] and anion$-\pi$[36] may also play an important role in their adhesion. This versatility of the adhesion of Mfps has generated significant interest in synthesizing polymers containing DOPA functionalities for biomedical and engineering applications.[37−44]

The Mfps contain a diverse array of nonpolar and polar amino acid building blocks.[45] We limited the scope of this study to understand only the effects of appending amino acids and aromatic and hydroxyl groups in interfacial adhesion. More specifically, we sought to understand questions such as "would the −OH groups on an aromatic ring show different adhesion strengths compared to the −OH groups on a non-aromatic structure?" Testing even this simple hypothesis and isolating the effect of a chemical functional group is not a trivial task because the experimental adhesion strength is affected by a multitude of factors other than the chemistry of the functional groups.[46] For example, the change in chemistry not only changes the interfacial interactions offered by the adhesive but also alters the bulk viscoelastic properties of the adhesive material. Thus, there are limited studies that demonstrate the effect of chemical groups on interfacial interactions, as decoupling the contribution of interfacial adhesion to the change in chemistry is experimentally challenging.

To overcome this shortcoming and address the role of aromatic and hydroxyl groups on interfacial adhesion, in this study, we have designed four different mussel-inspired polymers (MIPs) appended with phenylalanine (Phe), serine (Ser), tyrosine (Tyr), and DOPA. MIPs have two components that are kept constant—a long chain of hydrocarbon that

Received: April 4, 2021
Revised: May 19, 2021
Published: June 3, 2021

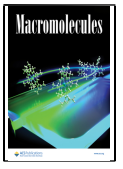

https://doi.org/10.1021/acs.macromol.1c00742
Macromolecules 2021, 54, 5417−5428

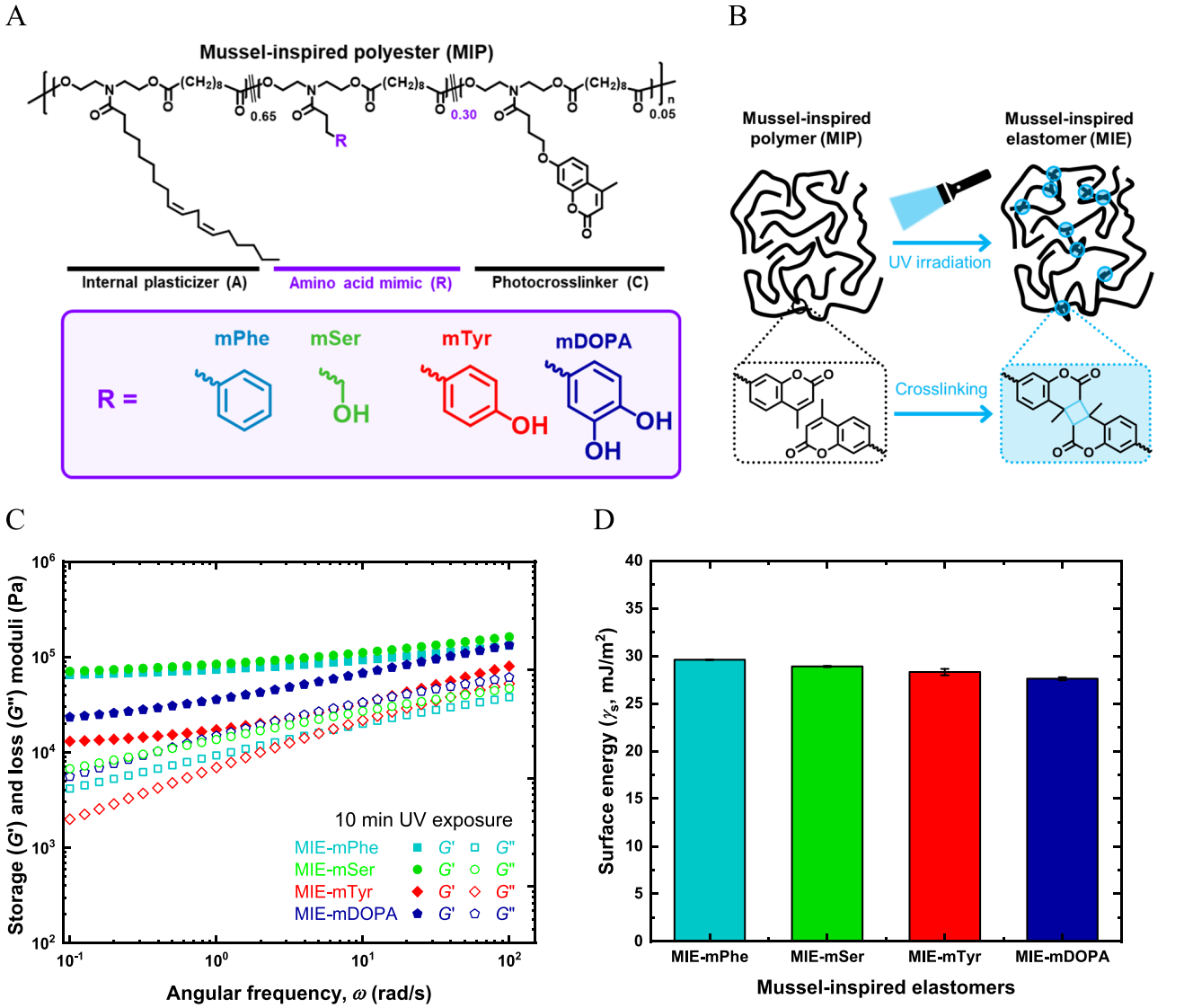

Figure 1. (A) Schematic representation of the Mfp-inspired polyesters (MIPs) synthesized to identify the consequences of functional group chemistry on the macroscopic interfacial adhesion. Four different statistical copolyesters were synthesized with mPhe, mSer, mTyr, and mDOPA pendant groups. The details of the synthesis are provided in the Supporting Information. (B) Graphical representation of the photocross-linking reaction of coumarin that leads to the formation of mussel-inspired elastomers (MIEs) from MIPs. (C) Storage (G') and loss (G'') moduli as a function of angular frequency (ω) obtained from the small-amplitude oscillatory shear (SAOS) measurements of the MIEs created by 10 min of photoirradiation of MIPs at 25 °C. (D) Surface energy (γ_S) of the MIEs was determined from the contact angle measurements of three liquids (water, ethylene glycol, and propylene glycol) on MIE films.

lowers the glass-transition temperature (T_g) and another component that provides cross-linking chemistry and reduces the viscoelastic dissipation.[47−49] With this polymer design, we have previously shown that a short UV exposure is enough to cross-link and generate a low modulus adhesive elastomer (MIE).[48] Four functional groups were chosen to test the contributions of the aromatic group (MIE-mPhe), −OH group (MIE-mSer), a single −OH attached to the aromatic group (MIE-mTyr), and two hydroxyl groups attached to a single aromatic group—the molecule expected to show the highest adhesion (MIE-mDOPA). The adhesion strength of MIEs was measured in contact with a plasma-treated glass substrate using Johnson−Kendall−Roberts (JKR) geometry. JKR geometry helps in reducing the contribution of viscoelastic effects from the measured adhesion during the pull-off cycle.[50]

We have used surface-sensitive sum-frequency generation (SFG) spectroscopy to measure the strength of the acid−base interactions (hydrogen bonding is a subset of acid−base interactions). In previous SFG experiments, we have demonstrated that the sapphire surface −OH group peak ($-OH_{sap}$) shift is directly correlated to the strength of the acid−base interactions between the $-OH_{sap}$ and the interacting groups.[51,52] The shifts of the $-OH_{sap}$ peak can be directly related to the interfacial enthalpic interactions.[48,53−59] We have used this approach to measure the enthalpy of interaction between $-OH_{sap}$ and model compounds that represent the four functionalities of interest—Phe, Ser, Tyr, and DOPA. To relate the enthalpic contribution to the work of adhesion, we need information on the interaction strength and the number of acid−base interactions with the surface OH_{sap}. The interaction strength and the number of interactions were determined by SFG and MD molecular dynamics (MD) simulations, respectively.[60−62] Based on the MD and SFG results, we calculated the trend expected for the adhesion for

https://doi.org/10.1021/acs.macromol.1c00742
Macromolecules 2021, 54, 5417−5428

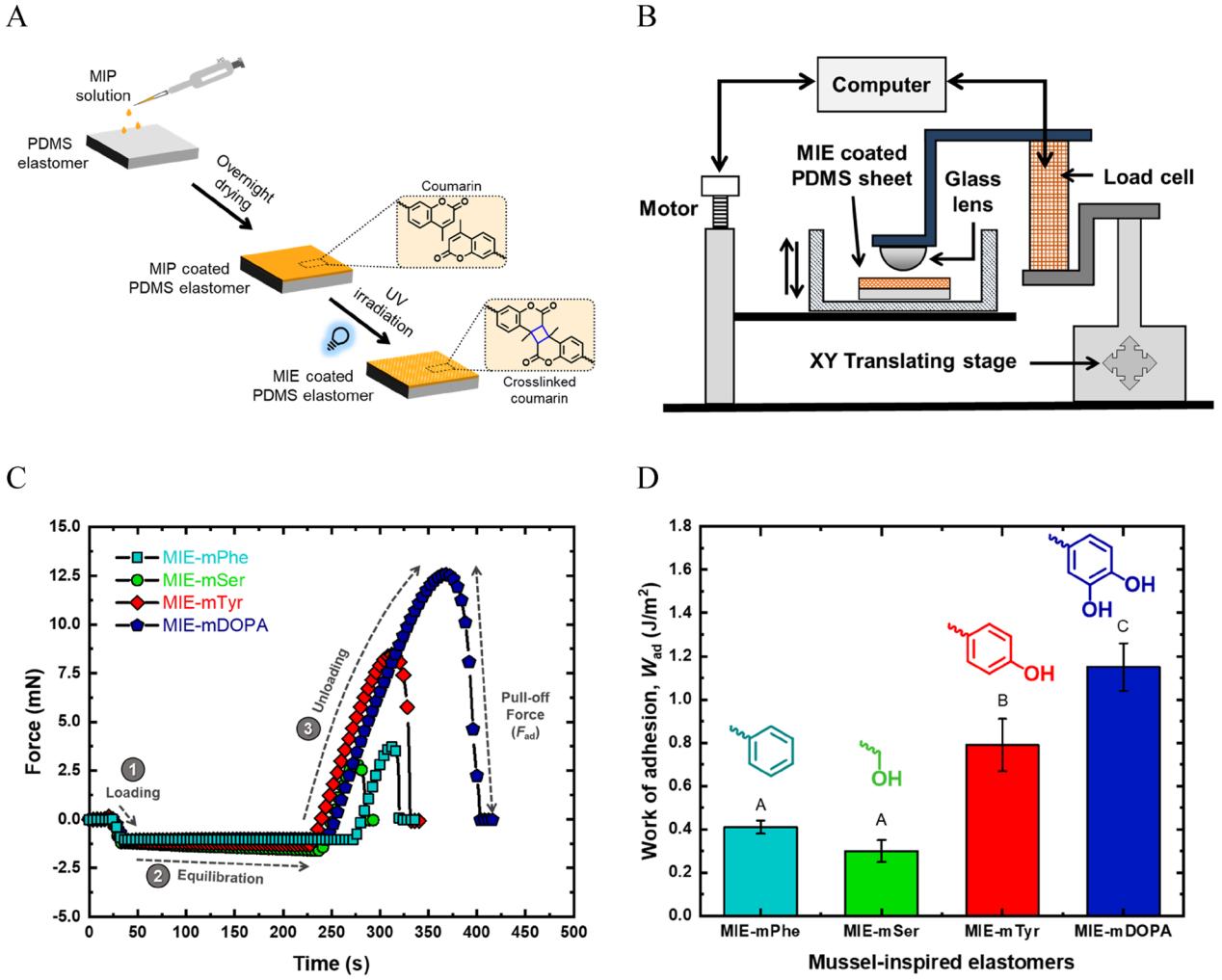

Figure 2. (A) Schematic diagram of the sample preparation for adhesion measurements. A thin layer of MIEs was deposited on top of a PDMS elastomer film. (B) Schematic representation of the instrument used for measuring the contact adhesion of a glass lens against the MIEs. (C) Representative force−distance curves were obtained during the measurement of contact adhesion between the hemispherical glass lens and MIEs. The rate of loading and unloading was 0.4 μm/s. The adhesive contacts were equilibrated under a preload of −1.0 mN for 5 min before the unloading experiments. (D) Work of adhesion (W_{ad}) of the MIEs was calculated from the pull-off forces using the JKR equation (eq 2). The data represented in the above plots are the average of five readings, and the error bars represent their standard deviation. The Tukey mean comparison test was used for identifying the statistical significance across the W_{ad} of MIEs. The differences in the alphabets above individual columns describe the statistical significance with $p < 0.05$.

the four different amino acid representative molecules. The comparison between the predicted and empirical results reveals not only the importance of the OH groups forming strong acid−base interactions with $-OH_{sap}$ but also the cumulative effect of multivalent weaker acid−base interactions between the aromatic group and the $-OH_{sap}$.

The synergy of the strong and weak acid−base interactions makes the DOPA functionality unique in forming a strong adhesive bond with hydroxyl-rich surfaces. Our integrative approach of tailored chemistry, interface-sensitive spectroscopy, and simulation provided a semi-empirical relationship between the molecular structure of Mfp-inspired nonionic functional groups and macroscopic adhesion strength. The results accurately identify the critical role of molecular orientations at the interface and the cumulative effect of multiple weak acid−base interactions in the experimentally observed adhesion strength.

RESULTS AND DISCUSSION

We have divided this section into five subsections. In the first subsection, the design of MIEs with four different functional groups and the results from the adhesion measurements are explained. In the second subsection, we describe the small molecule studies using SFG to determine the interaction enthalpy of the model compounds with $-OH_{sap}$. The third subsection details the MD results to calculate the molecular orientation and number of weak and strong acid−base interactions. In the fourth subsection, the prediction of work of adhesion per molecule using the results from SFG and MD simulations is described. Finally, in the fifth subsection, we discuss the implications of the results and describe some of the unresolved questions.

Design of the MIEs and Their Macroscopic Adhesion Measurements. To create adhesive elastomers with Mfp-inspired functional groups, four different mussel-inspired statistical copolyesters (MIPs, Figure 1A) were synthesized using a previously described polyesterification reaction

https://doi.org/10.1021/acs.macromol.1c00742
Macromolecules 2021, 54, 5417−5428

between three *N*-functionalized diethanolamide monomers (diols) and sebacic acid (dicarboxylic acid) (Scheme S2A).[47−49,63] Among the three diols, two of the diols (A and C) were incorporated in all four MIPs and the pendant group of the third diol monomer was varied (R) across the MIPs. First, a coumarin-functionalized diol monomer (C) was added in the MIPs at a constant feed ratio of 5 mol %. Coumarin undergoes [2 + 2] photocycloaddition upon exposure to light of wavelength, λ = 340 nm, providing chemically cross-linked elastomeric materials (Figure 1B).[47,49,64,65] An aliphatic diol (A) with nonpolar hydrocarbons was added at a feed ratio of 65 mol % to obtain elastomers with low moduli (internal plasticizer) after the cross-linking reaction of coumarin units. This unit also lowers the glass-transition temperatures of the MIPs.[66] Finally, to create MIPs with a variable number of aromatic and hydroxyl groups per monomer units, diols mimicking phenylalanine (mPhe, aromatic and no hydroxyl), serine (mSer, non-aromatic and one hydroxyl), tyrosine (mTyr, aromatic and one hydroxyl), and 3,4-dihydroxyphenylalanine (mDOPA, aromatic and two hydroxyls) were incorporated in the polyesters to obtain MIP-mPhe, MIP-mSer, MIP-mTyr, and MIP-mDOPA, respectively. A detailed description of the synthesis of amino acid mimetic diols (R) (Scheme S1) and polyesterification reactions (Scheme S2A) are provided in the Supporting Information. The analysis of the ^{1}H NMR (Figure S3) shows that the molar ratios of the three diols are similar across all MIPs. The molar masses of MIPs ($M_{n,GPC}$) were in the same range (Table S1).

The MIPs were photocross-linked by UV irradiation at λ = 340 nm to create the corresponding mussel-inspired elastomers (MIEs). These MIEs were used to examine the molecular origins of macroscopic adhesion of elastomers to a sapphire substrate. The viscoelastic properties of the MIEs were analyzed using small-amplitude oscillatory shear measurements (SAOS). The detailed procedure is provided in the Supporting Information. The MIEs were subjected to oscillatory shear at an angular frequency (ω) $\approx$ 0.1 to 100 rad/s, and the storage (G') and loss (G'') moduli were determined (Figure 1C). All the MIEs after exposure to UV-A show $G' > G''$, indicating the solid-like behavior at $\omega \approx$ 0.1 to 100 rad/s (Figure 1C). At low ω, both G' (13−71 k Pa) and G'' (2−7 kPa) show a similar range of values across the MIEs. The negligible variations in G' and G'' across the MIEs indicate the minimal effect of the structure of the R groups on bulk viscoelastic properties of the cross-linked networks. A detailed comparison of the rheological properties of the MIEs can be found in the Supporting Information. The similarities of MIPs in molar mass and the molar ratio of monomers and the R-group independent cross-linking chemistry provide MIEs with similar rheological properties.

The surface energy of MIEs was characterized by measuring the contact angle of three solvents (ethylene glycol, propylene glycol, and water) on thin films (thickness of ∼200 nm) of MIEs (details in the Supporting Information).[49,67] Figure 1D shows that all MIEs have a surface energy (γ_S) of ∼28 mJ/m^2.

The thermodynamic work of adhesion ($W_{ad(0)}$) is defined using eq 1, where γ_{12} is the interfacial energy between substrate 1 and 2 and γ_1 and γ_2 are the surface energies of the two substrates (eq 1).[68]

$$W_{ad(0)} = \gamma_1 + \gamma_2 - \gamma_{12} \tag{1}$$

The measured macroscopic adhesion strength has contributions from both the thermodynamic work of adhesion and bulk dissipation. Since the surface energies of the MIEs (γ_S) and substrate (γ_G, glass) and bulk rheological properties are almost similar across the MIEs (Figure 1C,D), the results from adhesion measurements will reflect the differences in the interfacial energy (γ_{SG}) at the contact interface between the MIEs and substrate.

Figure 2A shows the procedure for the fabrication of MIE-coated (thickness of ∼20 μm) PDMS films. The adhesion strength between the hemispherical glass lens (radius, R_l = 1.25 mm) and MIEs was measured using the JKR model pull-off adhesion test (rate of loading and unloading = 0.4 μm/s) using a home-built instrument (Figure 2B), described in detail elsewhere.[48] Figure 2C shows the representative force−distance curve and the pull-off force (F_{ad}) measurements. W_{ad} was calculated from F_{ad} using the following JKR equation:[50]

$$W_{ad} = \frac{F_{ad}}{1.5 \times \pi \times R_l} \tag{2}$$

Note that the values of W_{ad} reported here are much larger than those expected from eq 1 and include contributions due to either stretching of interfacial chains and (or) bulk dissipation.[46] Moreover, the W_{ad} determined from JKR geometry at low velocity is proportional (but not equal) to the thermodynamic work of adhesion ($W_{ad(0)}$).[50] We expect that the additional viscoelastic contributions are similar for all four systems, and we can attribute the variations in W_{ad} to the differences in their chemistries.

The subtle variations in the structure of pendant groups led to significant differences in the W_{ad} (Figure 2D). MIE-mDOPA (W_{ad} = 1.15 ± 0.11 J/m^2) showed the highest adhesion strength, while MIE-mPhe (W_{ad} = 0.41 ± 0.03 J/m^2) and MIE-mSer (W_{ad} = 0.30 ± 0.05 J/m^2) showed a relatively lower W_{ad}. Note that all the elastomers failed at the glass−elastomer interface (adhesive failure). To explain the trend in W_{ad}: MIE-mPhe < MIE-mTyr < MIE-mDOPA, we examined the interfacial interactions between model compounds and the hydroxylated surface.

Measurement of Interfacial Interactions of Model Compounds Using SFG. The sapphire surface (sapphire−air interface) has free hydroxyl groups (−OH$_{sap}$) that show a strong peak in the SFG spectra at ∼3700 to 3720 cm^{-1}. The location of this peak shifts to a lower wavenumber when in contact with other media. The enthalpy of interaction between −OH$_{sap}$ and the interacting molecules (ΔH_i) can be quantified from the shift in −OH$_{sap}$ vibration frequency ($\Delta\nu_i$) using the Badger−Bauer equation[69,70]

$$\Delta H_i = m\Delta\nu_i + c \tag{3}$$

where m and c are empirically determined constants for specific functional groups.

To examine the interfacial interactions between representative compounds and the sapphire (Al_2O_3) surface, the following molecules were selected: benzene (sm-Phe), methanol (sm-Ser), phenol (sm-Tyr), and catechol (sm-DOPA). These represent the pendant R groups of MIE-mPhe, MIE-mSer, MIE-mTyr, and MIE-mDOPA. The model molecules sm-Tyr and sm-DOPA are solids at room temperature. Therefore, sm-Tyr, sm-DOPA, and sm-Ser were dissolved in deuterated chloroform ($CDCl_3$) at a concentration of 0.07 M and injected into the SFG cell for this study (Figure 3A). In the case of sm-Phe, pure benzene was used for the SFG

https://doi.org/10.1021/acs.macromol.1c00742
Macromolecules 2021, 54, 5417−5428

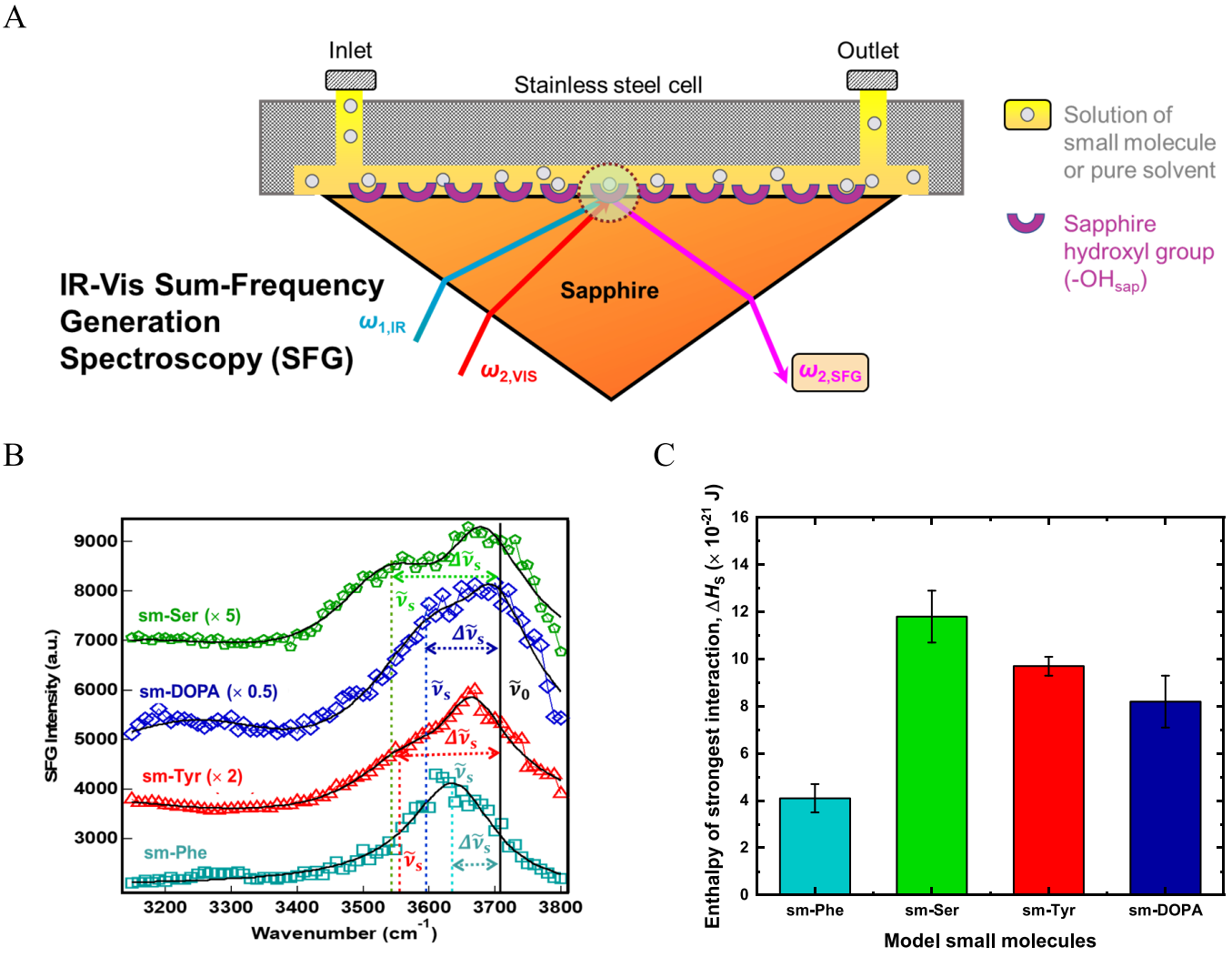

Figure 3. (A) Schematic of the SFG cell used for collecting the SFG spectra between model compounds and the sapphire surface. (B) SFG spectra (polarization: PPP) of the hydroxyl region ($-OH_{sap}$, 3100−3800 cm^{-1}) next to model compounds, representing amino acid mimetic groups conjugated in the MIEs. We have used benzene (sm-Phe), methanol (sm-Ser), phenol (sm-Tyr), and catechol (sm-DOPA) to represent mPhe, mSer, mTyr, and mDOPA, respectively. The spectra for sm-Ser, sm-Tyr, and sm-DOPA were collected from a 0.07 M solution of the respective molecule in $CDCl_3$. Pure benzene was used to collect the spectra of sm-Phe. (C) Highest $-OH_{sap}$ peak shift ($\Delta\tilde{\nu}_s = \tilde{\nu}_0 - \tilde{\nu}_s$) observed from SFG spectra was used for calculating the strongest interaction enthalpy ($\Delta H_s = m\,\Delta\nu_s + c$) using the Badger−Bauer equation (eq 3) for small molecule representatives next to sapphire.

experiment since the spectroscopic features at the $-OH_{sap}$ region of $CDCl_3$ and sm-Phe are similar. $CDCl_3$ was chosen as the solvent due to its ability to solubilize the small molecules and its weaker interaction with sapphire.[48]

Figure 3B shows the SFG spectra of the hydroxyl region after adsorption of sm-Phe, sm-Ser, sm-Tyr, and sm-DOPA. All spectra show a shift toward a lower wavenumber from the sapphire hydroxyl reference peak position at $\tilde{\nu}_0 \approx 3700\ cm^{-1}$ (free hydroxyl peak, the black solid line in Figure 3B). From the multipeak fitting analysis, the SFG spectra of sm-Ser, sm-Tyr, and sm-DOPA can be divided into two distributions. The first distribution (lower wavenumber, $\tilde{\nu}_S$) corresponds to the strongest interaction of $-OH_{sap}$ with the polar groups of the model compounds (hydrogen bonding interactions) and the second distribution (higher wavenumber, $\tilde{\nu}_w$) represents the weaker interactions of $-OH_{sap}$ with the less polar groups of the compounds or $CDCl_3$. The classification is based on the knowledge that the higher shift corresponds to stronger interactions and the strength of hydrogen bonding interaction is higher than other weak acid−base interactions.[69,71]

From the highest shifted peak, the enthalpy of the strongest interaction (ΔH_S) of the small molecules per $-OH_{sap}$ was calculated using eq 3 (Figure 3C). Two key observations were made from Figure 3C. First, sm-Ser showed the highest interaction enthalpy [$\Delta H_{S,\,sm-Ser} = (11.8 \pm 1.1) \times 10^{-21}$ J] compared to all other molecules. Second, sm-Phe had the lowest interaction strength [$\Delta H_{S,\,sm-Phe} = (4.1 \pm 0.6) \times 10^{-21}$ J], whereas both sm-Tyr [$\Delta H_{S,\,sm-Tyr} = (9.7 \pm 0.4) \times 10^{-21}$ J] and sm-DOPA [$\Delta H_{S,\,sm-DOPA} = (8.2 \pm 1.1) \times 10^{-21}$ J] showed a higher interaction strength than sm-Phe. Since W_{ad} is a function of molecular orientation and the number of interactions at the interface, in the next section, we discuss the MD simulation results to obtain these parameters.

Determination of the Orientation and Number of Interactions between the Model Compounds and $-OH_{sap}$ by MD Simulation. The MD simulations for a thin layer of model compounds in contact with the

https://doi.org/10.1021/acs.macromol.1c00742
Macromolecules 2021, 54, 5417−5428

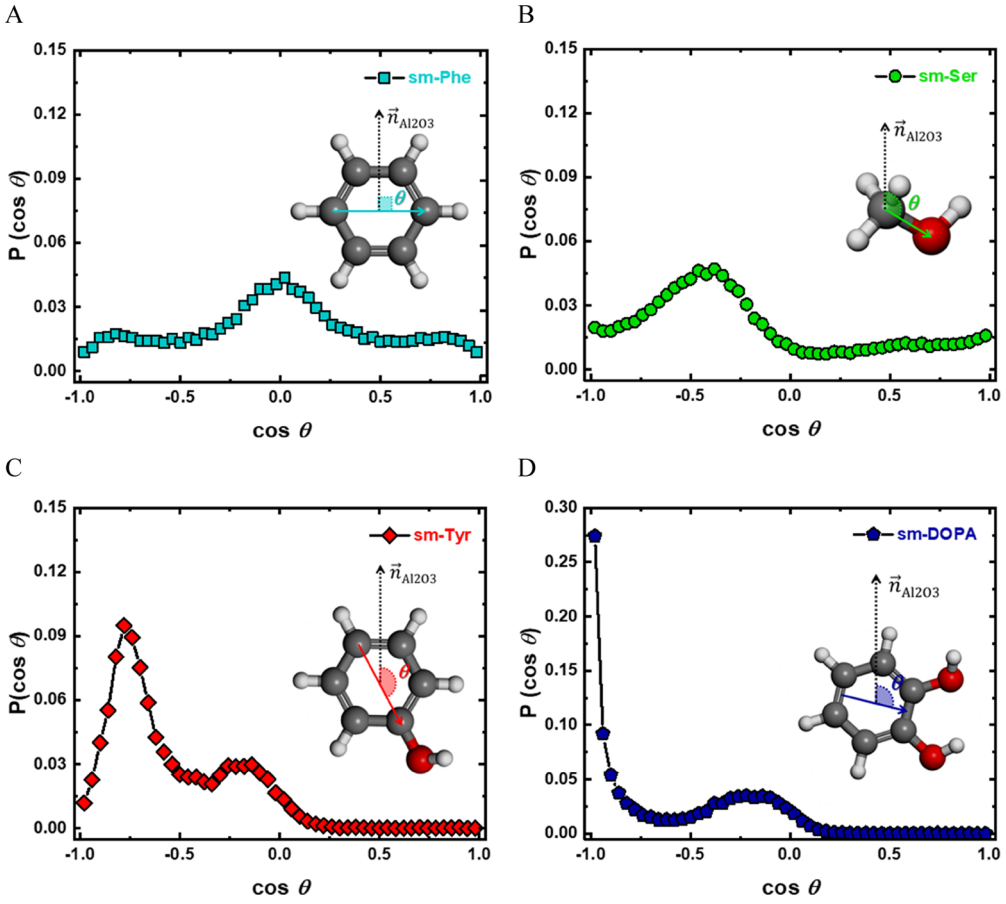

Figure 4. Summary of the molecular orientation of compounds representing different functional groups with respect to the hydroxylated α-Al_2O_3 surface calculated using MD simulations. Orientation distribution (probability of the cosines of the tilt angle, θ) of the bond vectors (as shown in the inset) with respect to the surface normal to the hydroxylated surface for (A) sm-Phe, (B) sm-Ser, (C) sm-Tyr, and (D) sm-DOPA. For (B) sm-Ser, (C) sm-Tyr, and (D) sm-DOPA, the model compounds were simulated as dilute solutions in chloroform. For (A) sm-Phe, pure benzene was used as a model liquid for the simulations. The systems were chosen to replicate the SFG spectroscopy experiments.

hydroxylated α-Al_2O_3 surface were performed (simulation methodology is described in the methods section of the Supporting Information). To replicate the SFG spectroscopy experiment, in the MD simulation, sm-Phe was simulated as pure benzene. The other compounds were simulated as dilute solutions in $CHCl_3$. Figure 4A–D shows the orientation distribution (probability of the cosines of the tilt angle, $P(\cos\theta)$) of the bond vectors with respect to the surface normal for sm-Phe, sm-Ser, sm-Tyr, and sm-DOPA (as shown in the inset). The distributions are plotted for the molecules in the interfacial layer. The interfacial layer was defined when the center of mass was within the first depletion region in atomic density profiles (Figure S5).[56] Azimuthal symmetry is assumed in all the plots. In bulk, the molecules are randomly orientated and have a constant $P(\cos\theta)$ value of 0.02 (for 50 bins used for plotting the data), suggesting equal probabilities for all the orientations.

For sm-Phe, the peak at $P(\cos\theta)$ is at $\cos\theta \approx 0$, suggesting that the sm-Phe bond vector lies parallel to the hydroxylated substrate. Further, the orientation distribution of the normal vector to the plane of the aromatic ring depicts that it is lying flat on the hydroxylated substrate (Figure S6). The flat configuration of sm-Phe provides the highest projected area on the hydroxylated surface, which illustrates that the benzene molecule tends to interact with multiple hydroxyl groups. The tilt angle orientation distribution of sm-Ser shows a peak at $\cos\theta \approx -0.54$ ($\theta = 123°$), displaying that the C–O bond vectors point toward the hydroxyl groups. The hydroxyl group in sm-Ser can form hydrogen bonds with the hydroxylated surface to maximize the enthalpic interactions and this explains the observed orientation. Notably, the tilt angle orientation distributions of both sm-Tyr and sm-DOPA exhibited two peaks (Figure 4C,D). In the case of sm-Tyr, the peaks were observed at $\cos\theta \approx -0.78$ and -0.14, whereas sm-DOPA displayed peaks at $\cos\theta \approx -1.0$ and -0.18. The observation of two peaks in the orientation distribution has been reported previously.[57] The interplay between the dipolar, dispersive, and hydrogen bonding interactions at the interface often leads to two or more probable molecular orientations.[56] For example, the peak at lower $\cos\theta$ (-0.78 for sm-Tyr and -1 for sm-DOPA) configurations originates from the near perpendicular orientation of the molecule through which the hydrogen bonds can be formed at the interfaces. Meanwhile, the broader peaks at higher $\cos\theta$ (-0.14 for sm-Tyr and -0.18 for sm-DOPA) correspond to the orientation where the planar aromatic groups (Figure S6) interact with the hydroxylated surface through weaker acid–base interactions. The MD results are consistent with previous simulation studies.[72]

The simulation results were further analyzed to find the type (i) and the number of interactions (n_i) that these compounds make with the surface hydroxyl groups. The average number of hydrogen bonds through the hydroxyl groups of the molecules

https://doi.org/10.1021/acs.macromol.1c00742
Macromolecules 2021, 54, 5417–5428

is obtained using the geometric criteria suggested by Luzar and Chandler.[73] Additionally, the van der Waals projected area is calculated from the molecular size of the benzene ring and the average of cos θ normal to the benzene ring (Figure S6).[74] Further, the projected area and the surface hydroxyl group density were utilized to calculate the number of acid−base interactions with the aromatic part of the molecule.

The sm-Phe molecule does not form hydrogen bonds since it lacks electronegative atoms. However, the aromatic group engages in weak acid−base interactions between the π electron cloud and sapphire hydroxyl groups.[58] The average number of acid−base interactions between different molecules through the aromatic and hydroxyl groups is summarized in Table 1.

Table 1. Summary of the Number of Interactions Displayed by the Small Molecules to the Hydroxylated α-Al_2O_3 Surface[b]

	no. of sapphire hydroxyl groups interacting with the hydroxyl or aromatic group(s) of the molecule	
molecule	hydroxyl groups	aromatic groups[a]
sm-Phe	0	4.60
sm-Ser	1.13	0
sm-Tyr	1.11	3.68
sm-DOPA	2.24	3.70

[a]The interaction numbers through aromatic groups were calculated considering the average of the normal to the aromatic group plane vector distributions (Figure S6) at the interface and the projected van der Waals area of the flat benzene ring. [b]The results are obtained from the MD simulations.

We observed that the aromatic groups of sm-Phe, sm-Tyr, and sm-DOPA interact through weak acid−base interactions with ∼4.6, 3.7, and 3.7 surface hydroxyl groups, respectively. Meanwhile, the hydroxyl groups of sm-Ser, sm-Tyr, and sm-DOPA form ∼1.1, 1.1, and 2.2 hydrogen bonds, respectively with the hydroxylated surface.

Combining SFG and MD Simulations to Calculate Overall Interaction Enthalpy. The overall interaction enthalpy of a molecule with surface hydroxyl groups ($\Delta H_{molecule}$) is the sum of the individual weak and strong acid−base interactions.[60,61] The determination of the type of interactions (i), number of interactions (n_i), and enthalpy of a single interaction (ΔH_i) enables the calculation of $\Delta H_{molecule}$ as described below.[60,62] ΔH_i can be obtained experimentally from SFG spectroscopy, and n_i can be calculated from MD simulations.[57,58]

$$\Delta H_{molecule} = \sum_i n_i \times \Delta H_i \quad (4)$$

The overall interaction enthalpy between the model small molecules and hydroxylated Al_2O_3 surface ($\Delta H_{molecule}$) was calculated using eq 4. For sm-Tyr and sm-DOPA, two different types of interactions were present, a weaker acid−base interaction between surface hydroxyl groups and aromatic groups ($-OH_{sap}\cdots-\pi_{sm}$) and the hydrogen bonds between surface hydroxyl groups and phenolic hydroxyl groups ($-OH_{sap}\cdots-OH_{sm}$). In such cases, the number of interactions through the specific group was multiplied by the respective interaction enthalpy per surface hydroxyl group. For determining the interaction enthalpy between the aromatic group and surface hydroxyl group, $\Delta H_{S,\ sm-Phe}$ (Figure 3C) was used for sm-Phe, sm-Tyr, and sm-DOPA. As the aromatic groups engage in weak acid−base interactions, the interaction enthalpies are low, and any small variation in the values (across sm-Phe, sm-Tyr, and sm-DOPA) would not change the results. For the hydroxyl groups, the interactions enthalpy per surface hydroxyl group of respective molecules was used. For example, in the case of sm-Tyr, the ΔH_i between aromatic and sapphire hydroxyl groups was $\sim(4.1 \pm 0.6) \times 10^{-21}$ J ($\sim\Delta H_{S,\ sm-Phe}$), and the ΔH_i between phenol hydroxyl group and sapphire hydroxyl group was $\sim(9.7 \pm 0.4) \times 10^{-21}$ J ($\Delta H_{S,\ sm-Tyr}$). There are ∼3.7 of the first type of interactions and ∼1.1 of the latter type interactions between sm-Tyr and the surface. Thus, the interaction per sm-Tyr molecule, $\Delta H_{molecule,\ sm-Tyr}$ determined from eq 4 was found to be $\sim(25.8 \pm 2.7) \times 10^{-21}$ J. Figure 5 presents a histogram of the calculated overall interaction enthalpy per molecule. The interaction enthalpy per molecule ($\Delta H_{molecule}$) followed the trend sm-DOPA > sm-Tyr > sm-Phe ≈ sm-Ser. Interestingly, the trend of W_{ad} (Figure 2D) is similar to the trends in $\Delta H_{molecule}$ (Figure 5).

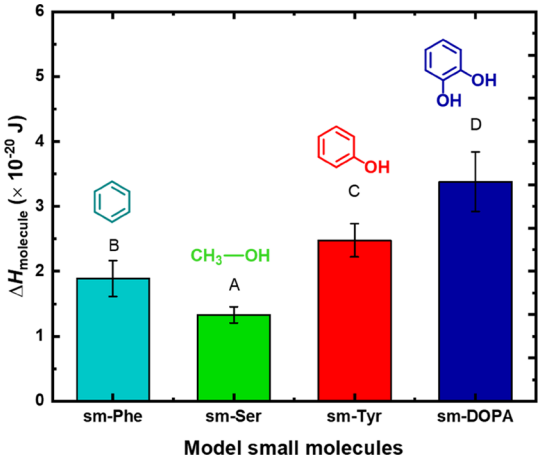

Figure 5. Overall interaction enthalpy ($\Delta H_{molecule}$) of the four compounds with $-OH_{sap}$ calculated using eq 4. Interaction enthalpies (ΔH_i) were obtained using the SFG data from Figure 3C and the number density from the MD simulations results in Table 1.

Implication of the Overlap between the Trends in W_{ad} and $\Delta H_{molecule}$ and Unresolved Questions. From eq 1, the thermodynamic work of adhesion between MIE and glass can be defined as follows:[68]

$$W_{ad(SG)} = \gamma_S + \gamma_G - \gamma_{SG} \quad (5)$$

In our study, the surface energies of MIEs are identical (γ_S, Figure 1D) and the substrate was constant (γ_G, glass). Therefore, the variation in the W_{ad} across the MIEs (Figure 2D) is due to their differences in interfacial energies between MIEs and glass (γ_{SG}). This is with the assumption that the viscoelastic contributions to the W_{ad} are similar across all four MIEs. Previously, our group has corroborated the actual thermodynamic work of adhesion ($W_{ad(0)}$) of small molecules with their γ_{SG} determined from SFG spectroscopy.[59] Based on this study, we anticipated that SFG spectroscopy will solely describe the trends of γ_{SG} in terms of ΔH_s. However, the ΔH_s obtained from SFG spectroscopy data did not align with the adhesion strength measurements of MIEs (Figure 6).

The MD simulation results show that the projected area on the substrate surface across the small molecule representatives is vastly different. The projected area of sm-Ser on the surface is lower than that of other molecules due to its smaller size and

https://doi.org/10.1021/acs.macromol.1c00742
Macromolecules 2021, 54, 5417−5428

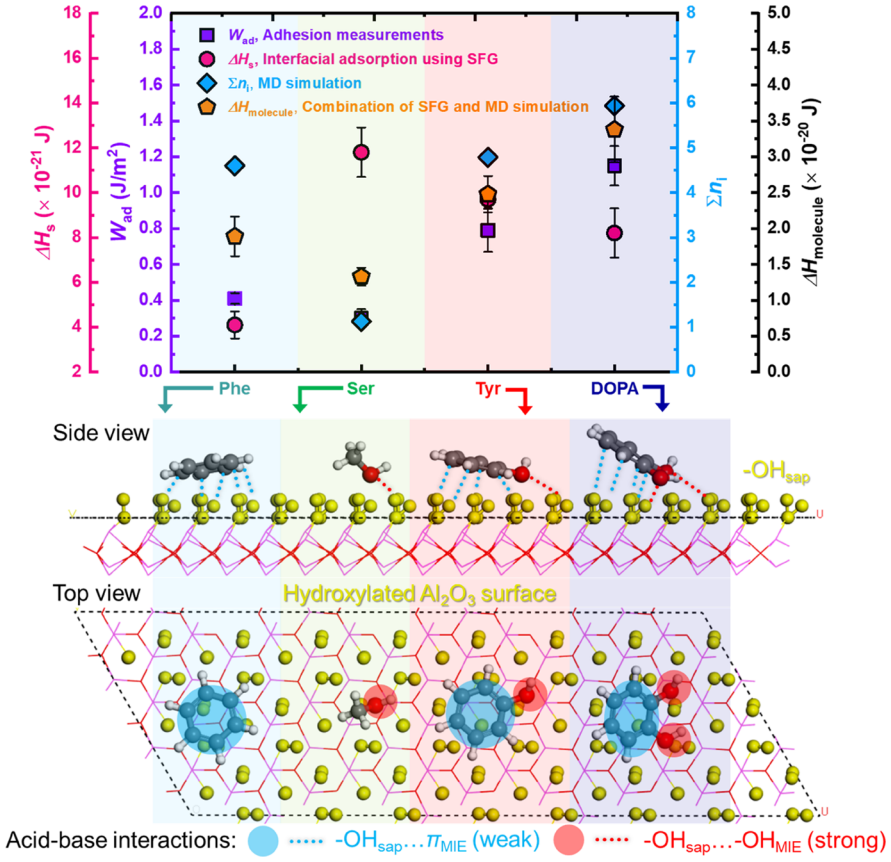

Figure 6. Adhesion mechanism of MIEs with hydroxylated surfaces. The macroscopic adhesion strength (W_{ad}, violet square) measured from the JKR model interfacial adhesion follows the trend of overall interaction enthalpy per molecule ($\Delta H_{molecule}$, orange pentagon) measured from the combination of SFG spectroscopy and MD simulations. A synergistic effect of the type of interaction (i), number of interactions (n_i), and their combined strength provide mussel-inspired functional groups their respective interfacial adhesion strength. The three-dimensional schematic of the bottom represents the interaction modes of the amino acid pendant groups to the hydroxylated Al_2O_3 surface. Both side (top) and top (bottom) views are drawn to visualize the orientation of the functional groups next to the surface. The dashed-line (side view) and circle (top view) shaded with sky blue represent the weak $-OH_{sap}\cdots-\pi_{MIE}$ interactions. The dashed-line (side view) and circle (top view) shaded with red represent strong $-OH_{sap}\cdots-OH_{MIE}$ interactions. Phe interacts with the surface using $-OH_{sap}\cdots-\pi_{MIE}$ only. Tyr and DOPA interact with the surface through both $-OH_{sap}\cdots-\pi_{MIE}$ and $-OH_{sap}\cdots-OH_{MIE}$.

perpendicular orientation (Figures 4A and 6). Meanwhile, the molecules with aromatic groups have a larger footprint on the surface and interact with a greater number of surface hydroxyl groups. For example, the catechol groups can interact simultaneously with ~6 hydroxyl groups on the surface with ~4 weaker acid−base interactions and ~2 strong hydrogen bonds.

The trends of interaction enthalpy per molecule ($\Delta H_{molecule}$) calculated from the combination of data from both SFG spectroscopy and MD simulation correlate with the macroscopic adhesion measurement results (Figure 6). The implications of this correlation are significant. First, it implies that the subtle changes in the chemistry of pendant functional groups have significant consequences in the overall interfacial adhesion. Second, the data from different functional groups show the importance of the interfacial orientation of the molecule, the strength of individual interactions, and the number of interactions. Finally, a cumulative effect of both the strength and number emerges to provide overall adhesion strength. These implications explain three key observations in the adhesion strength measurements. First, the similarity in the W_{ad} across MIE-mPhe and MIE-mSer shows that ~4.6 (multivalent) weak acid−base interactions ($-OH_{sap}\cdots-\pi_{MIE\text{-}mPhe}$) have the same effect as ~1.1 strong acid−base interaction ($-OH_{sap}\cdots-OH_{MIE\text{-}mSer}$). The second observation is that MIE-mTyr has a two-fold higher adhesion strength when compared to MIE-mPhe, although the total number of interactions in sm-Phe ($\Sigma n_i \approx 4.6$) and sm-Tyr ($\Sigma n_i \approx 4.8$) is similar. The increased W_{ad} of MIE-mTyr is a result of the strong $-OH_{sap}\cdots-OH_{MIE\text{-}mTyr}$ interactions that constitute ~25% of the total n_i, and 37% of $\Delta H_{molecule}$, which are absent in MIE-mPhe. Finally, the MIE-mDOPA showed the highest adhesion strength. The synergistic action of both multivalent weak (46% of $\Delta H_{molecule}$) and strong (54% of $\Delta H_{molecule}$) acid−base interactions provides the highest Σn_i and $\Delta H_{molecule}$, resulting in the highest W_{ad} for MIE-mDOPA.

The contribution of weak interactions between aromatic groups and the surface is often neglected in the literature.[13,21] The calculations of ΔH_s from SFG spectroscopy often neglect the weak interactions. We think that the mismatch between the trends in ΔH_s and $\Delta H_{molecule}$ originates from the omission of the contributions from weak interactions and the inability to accommodate n_i while calculating ΔH_s. Our results demonstrate that the weak acid−base interactions can play an equally important role as the strong interactions while determining the overall adhesion strength.

From AFM and SFA studies, the adhesion strength of DOPA-functionalized polymers to TiO_2 and mica surfaces has

https://doi.org/10.1021/acs.macromol.1c00742
Macromolecules 2021, 54, 5417−5428

Table 2. Summary of the $\Delta H_{molecule}$ and Their Percentage of Contributions from Weak ($-OH_{sap}\cdots-\pi_{sm}$) and Strong ($-OH_{sap}\cdots-OH_{sm}$) Acid−Base Interactions

		contribution of $\Delta H_{molecule}$ from	
molecule	$\Delta H_{molecule}$ ($\times 10^{-21}$ J)	$-OH_{sap}\cdots-\pi_{sm}$ (%)	$-OH_{sap}\cdots-OH_{sm}$ (%)
sm-Phe	18.9 ± 2.8	100	0
sm-Ser	13.3 ± 1.2	0	100
sm-Tyr	24.8 ± 2.6	63	37
sm-DOPA	33.8 ± 4.6	46	54

been reported to be greater than the corresponding Tyr or Phe variants.[13,23,24,75] It has been proposed that the ability of DOPA units to form coordination bonds to TiO_2 surfaces[13,21,22] and bidentate hydrogen bonds to mica surfaces[18,75] is the factor for the superior adhesion strength of DOPA-conjugated molecules. Another frequent observation discussed in the literature is the similarity in the adhesion strength across Tyr and Phe.[23,24] The inability of Phe and Tyr to form bidentate interactions to surfaces is proposed to be the reason for their identical adhesion strength. In our study, interestingly, MIE-mTyr (W_{ad} = 0.79 ± 0.12 J/m^2) showed a lower adhesion strength than MIE-mDOPA, and the adhesion strength of MIE-mTyr was two-fold higher than that of MIE-mPhe. Further studies on mica and TiO_2 surfaces are necessary to resolve this anomaly in these results. From Table 2, it is evident that the weaker $-OH_{sap}\cdots-\pi_{Tyr}$ (63%) contributes more to the overall strength of MIE-mTyr than a stronger $-OH_{sap}\cdots-OH_{Tyr}$ (37%) interaction, indicating the importance of emergent multivalent interactions in determining the overall adhesion strength.

We recognize that correlating the adhesive properties of an elastomer made from multifunctional units to thermodynamic interaction parameters derived from their smaller building blocks required some critical assumptions. Notably, the trend of W_{ad} did not correlate with the trend of $\Delta H_{molecule}$/unit area (Figure S7). The effect of the other molecules in the backbone and side chain of the MIPs is assumed to be negligible throughout our study. The differences in interaction between different variable groups and other common functional units across MIPs may influence the interfacial orientation of variable groups. For example, the interaction between coumarin and aromatic groups across MIE-mPhe and MIE-mDOPA can be different. Recently, it was shown that the subtle changes in functional groups in the polymer backbone can alter the adhesion behavior of synthetic polymers and proteins.[76,77]

In this study, the entropic constraints of the polymer chains are neglected during the simplification of polymers to small molecules. A consequence of this is the assumption that the interfacial segregation of functional groups across the MIEs be similar. One can imagine that the orientation of the small molecules when adsorbed to a surface could be different from when the molecules are tethered to a polymer. Despite the assumptions, it is interesting that the qualitative trends are captured by only considering the molecular repeat unit. In the future, an investigation using MD simulation with polymer chains is necessary to verify the implications of these assumptions.

CONCLUSIONS

In conclusion, by synthesizing MIEs appended with Phe, Ser, Tyr, and DOPA mimetic functional groups, we have addressed the role of aromatic and hydroxyl groups in influencing adhesion strength to surfaces with −OH groups. The JKR model adhesion strength measurement shows that the W_{ad} follows the trend: MIE-mDOPA > MIE-mTyr > MIE-mPhe ≈ MIE-mSer. We found that the adhesion strength does not correlate with the sequence of the strongest interaction enthalpy obtained from SFG spectroscopy (ΔH_s: sm-Ser > sm-Tyr > sm-DOPA > sm-Phe). Instead, both the numbers of strong and weak acid−base interactions with surface hydroxyl groups per molecule predict the trend in adhesion strength. For example, sm-Ser interacts with the surface exclusively through hydrogen bonding, whereas sm-Tyr and sm-DOPA interact with the surface using both weak acid−base interaction and hydrogen bonding.

The enthalpy of interaction per molecule ($\Delta H_{molecule}$) calculated from combining the results from both MD simulation and SFG spectroscopy correlates with W_{ad}. The coalescence of dual-modal (weak and strong interactions), multivalent interactions of aromatic and hydroxyl groups with surface hydroxyl groups provides higher adhesion strength for both MIE-mTyr and MIE-mDOPA. The additional hydroxyl group in the DOPA compared to Tyr brings ∼1.1 additional $-OH_{sap}\cdots-OH_{MIE}$ interactions to MIE-mDOPA compared to MIE-mTyr, leading to the higher W_{ad} of MIE-mDOPA. The study depicts an effective identification of molecular parameters that govern the macroscopic adhesion behavior of elastomers. This understanding can help guide us in developing stronger adhesives by designing molecular units that can synergistically use both strong and weak acid−base interactions to increase the adhesion strengths.

ASSOCIATED CONTENT

Supporting Information

The Supporting Information is available free of charge at https://pubs.acs.org/doi/10.1021/acs.macromol.1c00742.

Experimental section with details on the materials, instrumentation, and synthetic procedures of monomers, polymers, and deprotection reactions; schematic representation of the monomer synthesis, polymerization, and deprotection reactions (Schemes S1 and S2); ^{1}H NMR of the mSer-TBDMS and mTyr-MEM monomers (Figures S1 and S2); ^{1}H NMR of the MIPs (Figure S3); summary of the molecular characterization of the MIPs (Table S1); details of the procedures of rheology, surface energy, SFG, and MD simulation experiments; plot generated for calculating surface energy of MIEs (Figure S4); density profile of the center of mass (Figure S5) and orientation distribution (Figure S6) of the small molecules obtained from MD simulations; $\Delta H_{molecule}$ per unit area of the small molecule representatives (Figure S7) (PDF)

https://doi.org/10.1021/acs.macromol.1c00742
Macromolecules 2021, 54, 5417−5428

AUTHOR INFORMATION

Corresponding Authors

Abraham Joy − *School of Polymer Science and Polymer Engineering, The University of Akron, Akron, Ohio 44325, United States;* orcid.org/0000-0001-7781-3817; Email: abraham@uakron.edu

Ali Dhinojwala − *School of Polymer Science and Polymer Engineering, The University of Akron, Akron, Ohio 44325, United States;* orcid.org/0000-0002-3935-7467; Email: ali4@uakron.edu

Authors

Amal Narayanan − *School of Polymer Science and Polymer Engineering, The University of Akron, Akron, Ohio 44325, United States;* orcid.org/0000-0001-8159-6878

Sukhmanjot Kaur − *School of Polymer Science and Polymer Engineering, The University of Akron, Akron, Ohio 44325, United States*

Nityanshu Kumar − *School of Polymer Science and Polymer Engineering, The University of Akron, Akron, Ohio 44325, United States;* orcid.org/0000-0002-4655-4653

Mesfin Tsige − *School of Polymer Science and Polymer Engineering, The University of Akron, Akron, Ohio 44325, United States;* orcid.org/0000-0002-7540-2050

Complete contact information is available at: https://pubs.acs.org/10.1021/acs.macromol.1c00742

Author Contributions

[#]A.N. and S.K. contributed equally in this work.

Notes

The authors declare no competing financial interest.

ACKNOWLEDGMENTS

Authors acknowledge funding from the National Science Foundation (NSF) (DMR awards 1508440, DMR 1610483, and DMR 1912329), the University of Akron start-up funds, and the Ohio Soybean Council Foundation Graduate Scholarship 2016-17 (S.K.). The authors acknowledge Dr. Qianhui Liu, Dr. Siddhesh Dalvi, and Mr. Yen-Min Tseng for their assistance during the experiments.

REFERENCES

(1) Autumn, K.; Liang, Y. A.; Hsieh, S. T.; Zesch, W.; Chan, W. P.; Kenny, T. W.; Fearing, R.; Full, R. J. Adhesive Force of a Single Gecko Foot-Hair. *Nature* **2000**, *405*, 681−685.

(2) Geim, A. K.; Dubonos, S. V.; Grigorieva, I. V.; Novoselov, K. S.; Zhukov, A. A.; Shapoval, S. Y. Microfabricated Adhesive Mimicking Gecko Foot-Hair. *Nat. Mater.* **2003**, *2*, 461−463.

(3) Smith, A. M. The Structure and Function of Adhesive Gels from Invertebrates. *Integr. Comp. Biol.* **2002**, *42*, 1164−1171.

(4) Li, J.; Celiz, A. D.; Yang, J.; Yang, Q.; Wamala, I.; Whyte, W.; Seo, B. R.; Vasilyev, N. V.; Vlassak, J. J.; Suo, Z.; Mooney, D. J. Tough Adhesives for Diverse Wet Surfaces. *Science* **2017**, *357*, 378−381.

(5) Bond, J. E.; Opell, B. D. Testing Adaptive Radiation and Key Innovation Hypotheses in Spiders. *Evolution (N. Y).* **1998**, *52*, 403−414.

(6) Singla, S.; Amarpuri, G.; Dhopatkar, N.; Blackledge, T. A.; Dhinojwala, A. Hygroscopic Compounds in Spider Aggregate Glue Remove Interfacial Water to Maintain Adhesion in Humid Conditions. *Nat. Commun.* **2018**, *9*, 1890.

(7) Stewart, R. J.; Weaver, J. C.; Morse, D. E.; Waite, J. H. The Tube Cement of Phragmatopoma Californica: A Solid Foam. *J. Exp. Biol.* **2004**, *207*, 4727−4734.

(8) Shao, H.; Bachus, K. N.; Stewart, R. J. A Water-Borne Adhesive Modeled after the Sandcastle Glue of P. Californica. *Macromol. Biosci.* **2009**, *9*, 464−471.

(9) Waite, J. H.; Tanzer, M. L. Polyphenolic Substance of Mytilus Edulis: Novel Adhesive Containing L-Dopa and Hydroxyproline. *Science* **1981**, *212*, 1038−1040.

(10) Yamamoto, H. Synthesis and Adhesive Studies of Marine Polypeptides. *J. Chem. Soc. Perkin Trans. 1* **1987**, 613−618.

(11) Ahn, B. K. Perspectives on Mussel-Inspired Wet Adhesion. *J. Am. Chem. Soc.* **2017**, *139*, 10166−10171.

(12) Waite, J. H. Mussel Adhesion - Essential Footwork. *J. Exp. Biol.* **2017**, *220*, 517−530.

(13) Lee, H.; Scherer, N. F.; Messersmith, P. B. Single-Molecule Mechanics of Mussel Adhesion. *Proc. Natl. Acad. Sci. U. S. A.* **2006**, *103*, 12999−13003.

(14) Yu, J.; Wei, W.; Menyo, M. S.; Masic, A.; Waite, J. H.; Israelachvili, J. N. Adhesion of Mussel Foot Protein-3 to TiO2 Surfaces: The Effect of PH. *Biomacromolecules* **2013**, *14*, 1072−1077.

(15) Del Grosso, C. A.; Leng, C.; Zhang, K.; Hung, H. C.; Jiang, S.; Chen, Z.; Wilker, J. J. Surface Hydration for Antifouling and Bio-Adhesion. *Chem. Sci.* **2020**, *11*, 10367−10377.

(16) Chen, Y.; Meng, J.; Gu, Z.; Wan, X.; Jiang, L.; Wang, S. Bioinspired Multiscale Wet Adhesive Surfaces: Structures and Controlled Adhesion. *Adv. Funct. Mater.* **2020**, *30*, 1905287 (1-21).

(17) Lin, Q.; Gourdon, D.; Sun, C.; Holten-Andersen, N.; Anderson, T. H.; Waite, J. H.; Israelachvili, J. N. Adhesion Mechanisms of the Mussel Foot Proteins Mfp-1 and Mfp-3. *Proc. Natl. Acad. Sci. U. S. A.* **2007**, *104*, 3782−3786.

(18) Anderson, T. H.; Yu, J.; Estrada, A.; Hammer, M. U.; Waite, J. H.; Israelachvili, J. N. The Contribution of DOPA to Substrate-Peptide Adhesion and Internal Cohesion of Mussel-Inspired Synthetic Peptide Films. *Adv. Funct. Mater.* **2010**, *20*, 4196−4205.

(19) Danner, E. W.; Kan, Y.; Hammer, M. U.; Israelachvili, J. N.; Waite, J. H. Adhesion of Mussel Foot Protein Mefp-5 to Mica: An Underwater Superglue. *Biochemistry* **2012**, *51*, 6511−6518.

(20) Yu, J.; Kan, Y.; Rapp, M.; Danner, E.; Wei, W.; Das, S.; Miller, D. R.; Chen, Y.; Waite, J. H.; Israelachvili, J. N. Adaptive Hydrophobic and Hydrophilic Interactions of Mussel Foot Proteins with Organic Thin Films. *Proc. Natl. Acad. Sci. U. S. A.* **2013**, *110*, 15680−15685.

(21) Li, Y.; Qin, M.; Li, Y.; Cao, Y.; Wang, W. Single Molecule Evidence for the Adaptive Binding of DOPA to Different Wet Surfaces. *Langmuir* **2014**, *30*, 4358−4366.

(22) Li, Y.; Liu, H.; Wang, T.; Qin, M.; Cao, Y.; Wang, W. Single-Molecule Force Spectroscopy Reveals Multiple Binding Modes between DOPA and Different Rutile Surfaces. *ChemPhysChem* **2017**, *18*, 1466−1469.

(23) Das, P.; Reches, M. Revealing the Role of Catechol Moieties in the Interactions between Peptides and Inorganic Surfaces. *Nanoscale* **2016**, *8*, 15309−15316.

(24) Maier, G. P.; Rapp, M. V.; Waite, J. H.; Israelachvili, J. N.; Butler, A. Adaptive Synergy between Catechol and Lysine Promotes Wet Adhesion by Surface Salt Displacement. *Science* **2015**, *349*, 628−632.

(25) Rapp, M. V.; Maier, G. P.; Dobbs, H. A.; Higdon, N. J.; Waite, J. H.; Butler, A.; Israelachvili, J. N. Defining the Catechol-Cation Synergy for Enhanced Wet Adhesion to Mineral Surfaces. *J. Am. Chem. Soc.* **2016**, *138*, 9013−9016.

(26) Li, Y.; Liao, M.; Zhou, J. Catechol-Cation Adhesion on Silica Surfaces: Molecular Dynamics Simulations. *Phys. Chem. Chem. Phys.* **2017**, *19*, 29222−29231.

(27) Li, Y.; Wang, T.; Xia, L.; Wang, L.; Qin, M.; Li, Y.; Wang, W.; Cao, Y. Single-Molecule Study of the Synergistic Effects of Positive Charges and Dopa for Wet Adhesion. *J. Mater. Chem. B* **2017**, *5*, 4416−4420.

(28) Han, L.; Gong, L.; Chen, J.; Zhang, J.; Xiang, L.; Zhang, L.; Wang, Q.; Yan, B.; Zeng, H. Universal Mussel-Inspired Ultrastable Surface-Anchoring Strategy via Adaptive Synergy of Catechol and Cations. *ACS Appl. Mater. Interfaces* **2018**, *10*, 2166−2173.

(29) Zhang, C.; Xiang, L.; Zhang, J.; Gong, L.; Han, L.; Xu, Z. K.; Zeng, H. Tough and Alkaline-Resistant Mussel-Inspired Wet Adhesion with Surface Salt Displacement via Polydopamine/Amine Synergy. *Langmuir* **2019**, *35*, 5257−5263.
(30) Fan, H.; Wang, J.; Tao, Z.; Huang, J.; Rao, P.; Kurokawa, T.; Gong, J. P. Adjacent Cationic−Aromatic Sequences Yield Strong Electrostatic Adhesion of Hydrogels in Seawater. *Nat. Commun.* **2019**, *10*, 5127 (1-8).
(31) Degen, G. D.; Stow, P. R.; Lewis, R. B.; Andresen Eguiluz, R. C.; Valois, E.; Kristiansen, K.; Butler, A.; Israelachvili, J. N. Impact of Molecular Architecture and Adsorption Density on Adhesion of Mussel-Inspired Surface Primers with Catechol-Cation Synergy. *J. Am. Chem. Soc.* **2019**, *141*, 18673−18681.
(32) Lu, Q.; Danner, E.; Waite, J. H.; Israelachvili, J. N.; Zeng, H.; Hwang, D. S. Adhesion of Mussel Foot Proteins to Different Substrate Surfaces. *J. R. Soc., Interface* **2013**, *10*, 20120759 (1-11).
(33) Wei, W.; Yu, J.; Broomell, C.; Israelachvili, J. N.; Waite, J. H. Hydrophobic Enhancement of Dopa-Mediated Adhesion in a Mussel Foot Protein. *J. Am. Chem. Soc.* **2013**, *135*, 377−383.
(34) Lu, Q.; Oh, D. X.; Lee, Y.; Jho, Y.; Hwang, D. S.; Zeng, H. Nanomechanics of Cation-π Interactions in Aqueous Solution. *Angew. Chem., Int. Ed.* **2013**, *52*, 3944−3948.
(35) Gebbie, M. A.; Wei, W.; Schrader, A. M.; Cristiani, T. R.; Dobbs, H. A.; Idso, M.; Chmelka, B. F.; Waite, J. H.; Israelachvili, J. N. Tuning Underwater Adhesion with Cation-π Interactions. *Nat. Chem.* **2017**, *9*, 473−479.
(36) Zhang, J.; Xiang, L.; Yan, B.; Zeng, H. Nanomechanics of Anion-π Interaction in Aqueous Solution. *J. Am. Chem. Soc.* **2020**, *142*, 1710−1714.
(37) Hofman, A. H.; van Hees, I. A.; Yang, J.; Kamperman, M. Bioinspired Underwater Adhesives by Using the Supramolecular Toolbox. *Adv. Mater.* **2018**, *30*, 1704640. (1-38)
(38) Li, L.; Smitthipong, W.; Zeng, H. Mussel-Inspired Hydrogels for Biomedical and Environmental Applications. *Polym. Chem.* **2015**, *6*, 353−358.
(39) Balkenende, D. W. R.; Winkler, S. M.; Messersmith, P. B. Marine-Inspired Polymers in Medical Adhesion. *Eur. Polym. J.* **2019**, *116*, 134−143.
(40) Guo, Q.; Chen, J.; Wang, J.; Zeng, H.; Yu, J. Recent Progress in Synthesis and Application of Mussel-Inspired Adhesives. *Nanoscale* **2020**, *12*, 1307−1324.
(41) Westwood, G.; Horton, T. N.; Wilker, J. J. Simplified Polymer Mimics of Cross-Linking Adhesive Proteins. *Macromolecules* **2007**, *40*, 3960−3964.
(42) Matos-Pérez, C. R.; White, J. D.; Wilker, J. J. Polymer Composition and Substrate Influences on the Adhesive Bonding of a Biomimetic, Cross-Linking Polymer. *J. Am. Chem. Soc.* **2012**, *134*, 9498−9505.
(43) Meredith, H. J.; Jenkins, C. L.; Wilker, J. J. Enhancing the Adhesion of a Biomimetic Polymer Yields Performance Rivaling Commercial Glues. *Adv. Funct. Mater.* **2014**, *24*, 3259−3267.
(44) North, M. A.; Del Grosso, C. A.; Wilker, J. J. High Strength Underwater Bonding with Polymer Mimics of Mussel Adhesive Proteins. *ACS Appl. Mater. Interfaces* **2017**, *9*, 7866−7872.
(45) Seo, S.; Das, S.; Zalicki, P. J.; Mirshafian, R.; Eisenbach, C. D.; Israelachvili, J. N.; Waite, J. H.; Ahn, B. K. Microphase Behavior and Enhanced Wet-Cohesion of Synthetic Copolyampholytes Inspired by a Mussel Foot Protein. *J. Am. Chem. Soc.* **2015**, *137*, 9214−9217.
(46) Gent, A. N. Adhesion and Strength of Viscoelastic Solids. Is There a Relationship between Adhesion and Bulk Properties? *Langmuir* **1996**, *12*, 4492−4496.
(47) Xu, Y.; Liu, Q.; Narayanan, A.; Jain, D.; Dhinojwala, A.; Joy, A. Mussel-Inspired Polyesters with Aliphatic Pendant Groups Demonstrate the Importance of Hydrophobicity in Underwater Adhesion. *Adv. Mater. Interfaces* **2017**, *4*, 1700506. (1-6)
(48) Kaur, S.; Narayanan, A.; Dalvi, S.; Liu, Q.; Joy, A.; Dhinojwala, A. Direct Observation of the Interplay of Catechol Binding and Polymer Hydrophobicity in a Mussel-Inspired Elastomeric Adhesive. *ACS Cent. Sci.* **2018**, *4*, 1420−1429.
(49) Narayanan, A.; Kaur, S.; Peng, C.; Debnath, D.; Mishra, K.; Liu, Q.; Dhinojwala, A.; Joy, A. Viscosity Attunes the Adhesion of Bioinspired Low Modulus Polyester Adhesive Sealants to Wet Tissues. *Biomacromolecules* **2019**, *20*, 2577−2586.
(50) Johnson, K. L.; Kendall, K.; Roberts, A. D. Surface Energy and the Contact of Elastic Solids. *Proc. R. Soc. London. A. Math. Phys. Sci.* **1971**, *324*, 301−313.
(51) Lambert, A. G.; Davies, P. B.; Neivandt, D. J. Implementing the Theory of Sum Frequency Generation Vibrational Spectroscopy: A Tutorial Review. *Appl. Spectrosc. Rev.* **2005**, *40*, 103−145.
(52) Shen, Y. R. Surface Properties Probed by Second-Harmonic and Sum-Frequency Generation. *Nature* **1989**, *337*, 519−525.
(53) Kurian, A.; Prasad, S.; Dhinojwala, A. Direct Measurement of Acid-Base Interaction Energy at Solid Interfaces. *Langmuir* **2010**, *26*, 17804−17807.
(54) Prasad, S.; Zhu, H.; Kurian, A.; Badge, I.; Dhinojwala, A. Interfacial Segregation in Polymer Blends Driven by Acid-Base Interactions. *Langmuir* **2013**, *29*, 15727−15731.
(55) Zhu, H.; Dhopatkar, N.; Dhinojwala, A. Effect of Acid-Base Interactions on Conformation of Adsorbed Polymer Chains. *ACS Macro Lett.* **2016**, *5*, 45−49.
(56) Kumar, N.; Singla, S.; Wilson, M. C.; Kaur, S.; Bekele, S.; Tsige, M.; Dhinojwala, A. Atomistic Insights into Hydrogen-Bonding-Driven Competitive Adsorption of Acetone-Chloroform Binary Mixtures. *J. Phys. Chem. C* **2019**, *123*, 29729−29738.
(57) Kumar, N.; Kaur, S.; Kumar, R.; Wilson, M. C.; Bekele, S.; Tsige, M.; Dhinojwala, A. Interaction Geometry Causes Spectral Line-Shape Broadening at the Solid/Liquid Interface. *J. Phys. Chem. C* **2019**, *123*, 30447−30457.
(58) Wilson, M. C.; Singla, S.; Stefin, A. J.; Kaur, S.; Brown, J. V.; Dhinojwala, A. Characterization of Acid-Base Interactions Using Interface-Sensitive Sum Frequency Generation Spectroscopy. *J. Phys. Chem. C* **2019**, *123*, 18495−18501.
(59) Singla, S.; Wilson, M. C.; Dhinojwala, A. Spectroscopic Evidence for Acid-Base Interaction Driven Interfacial Segregation. *Phys. Chem. Chem. Phys.* **2019**, *21*, 2513−2518.
(60) Fowkes, F. M. Role of Acid-Base Interfacial Bonding in Adhesion. *J. Adhes. Sci. Technol.* **1987**, *1*, 7−27.
(61) Chaudhury, M. K.; Whitesides, G. M. Correlation between Surface Free Energy and Surface Constitution. *Science* **1992**, *255*, 1230−1232.
(62) Chaudhury, M. K. Interfacial Interaction between Low-Energy Surfaces. *Mater. Sci. Eng. R Rep.* **1996**, *16*, 97−159.
(63) Gokhale, S.; Xu, Y.; Joy, A. A Library of Multifunctional Polyesters with "Peptide-Like" Pendant Functional Groups. *Biomacromolecules* **2013**, *14*, 2489−2493.
(64) Narayanan, A.; Xu, Y.; Dhinojwala, A.; Joy, A. Advances in Photoreactive Tissue Adhesives Derived from Natural Polymers. *ChemEngineering* **2020**, *4*, 32.
(65) Narayanan, A.; Menefee, J. R.; Liu, Q.; Dhinojwala, A.; Joy, A. Lower Critical Solution Temperature-Driven Self-Coacervation of Nonionic Polyester Underwater Adhesives. *ACS Nano* **2020**, *14*, 8359−8367.
(66) Liu, X.; Jain, T.; Liu, Q.; Joy, A. Structural Insight into the Viscoelastic Behaviour of Elastomeric Polyesters: Effect of the Nature of Fatty Acid Side Chains and the Degree of Unsaturation. *Polym. Chem.* **2020**, *11*, 5216−5224.
(67) Owens, D. K.; Wendt, R. C. Estimation of the Surface Free Energy of Polymers. *J. Appl. Polym. Sci.* **1969**, *13*, 1741−1747.
(68) Dupré, A.; Dupré, P. *Théorie Mécanique de La Chaleur*; Gauthier-Villars, 1869.
(69) Badger, R. M.; Bauer, S. H. Spectroscopic Studies of the Hydrogen Bond. II. The Shift of the O-H Vibrational Frequency in the Formation of the Hydrogen Bond. *J. Chem. Phys.* **1937**, *5*, 839−851.
(70) Joesten, M. D.; Drago, R. S. The Validity of Frequency Shift-Enthalpy Correlations. I. Adducts of Phenol with Nitrogen and Oxygen Donors. *J. Am. Chem. Soc.* **1962**, *84*, 3817−3821.

https://doi.org/10.1021/acs.macromol.1c00742
Macromolecules 2021, 54, 5417−5428

(71) Fowkes, F. M. Attractive Forces At Interfaces. *Ind. Eng. Chem.* **1964**, *56*, 40−52.
(72) Yeh, I. C.; Lenhart, J. L.; Rinderspacher, B. C. Molecular Dynamics Simulations of Adsorption of Catechol and Related Phenolic Compounds to Alumina Surfaces. *J. Phys. Chem. C* **2015**, *119*, 7721−7731.
(73) Luzar, A.; Chandler, D. Structure and Hydrogen Bond Dynamics of Water-Dimethyl Sulfoxide Mixtures by Computer Simulations. *J. Chem. Phys.* **1993**, *98*, 8160−8173.
(74) Webster, C. E.; Drago, R. S.; Zerner, M. C. Molecular Dimensions for Adsorptives. *J. Am. Chem. Soc.* **1998**, *120*, 5509−5516.
(75) Wei, W.; Yu, J.; Gebbie, M. A.; Tan, Y.; Martinez Rodriguez, N. R.; Israelachvili, J. N.; Waite, J. H. Bridging Adhesion of Mussel-Inspired Peptides: Role of Charge, Chain Length, and Surface Type. *Langmuir* **2015**, *31*, 1105−1112.
(76) Mu, Y.; Wu, X.; Pei, D.; Wu, Z.; Zhang, C.; Zhou, D.; Wan, X. Contribution of the Polarity of Mussel-Inspired Adhesives in the Realization of Strong Underwater Bonding. *ACS Biomater. Sci. Eng.* **2017**, *3*, 3133−3140.
(77) Wonderly, W. R.; Cristiani, T. R.; Cunha, K. C.; Degen, G. D.; Shea, J.-E.; Waite, J. H. Dueling Backbones: Comparing Peptoid and Peptide Analogues of a Mussel Adhesive Protein. *Macromolecules* **2020**, *53*, 6767−6779.

https://doi.org/10.1021/acs.macromol.1c00742
Macromolecules 2021, 54, 5417−5428